Supporting information for:

On-surface Synthesis of Rylene-type Graphene Nanoribbons

Haiming Zhang,[1,2] Haiping Lin,[1] Kewei Sun,[1] Long Chen,[3,4] Yulian Zagranyarski,[3] Nabi Aghdassi,[1] Steffen Duhm,[1] Qing Li,[1] Dingyong Zhong,[2,5] Youyong Li,[1] Klaus Müllen,[3*] Harald Fuchs[2*] and Lifeng Chi[1*]

1. *Jiangsu Key Laboratory for Carbon Based Functional Materials & Devices and Institute of Functional Nano & Soft Materials (FUNSOM), Soochow University, Suzhou 215123, P. R. China*
2. *Physikalisches Institut, Universität Münster, Wilhelm-Klemm-strasse 10, 48149 Münster, Germany and Center for Nanoscience and Technology (CeNTech), Heisenbergstrasse 11, 48149 Münster, Germany*
3. *Max Planck Institute for Polymer Research, 55124 Mainz, Germany*
4. *Department of Chemistry, School of Science, Tianjin University, and Collaborative Innovation Center of Chemical Science and Engineering, Tianjin 300072, China*
5. *School of Physics and Engineering & State Key Laboratory of Optoelectronic Materials and Technologies, Sun Yat-sen University, Xingang Xi Road 135, 510275 Guangzhou,China*

*Corresponding author, Email: chilf@suda.edu.cn, muellen@mpip-mainz.mpg.de, fuchsh@uni-muenster.de.

Experimental Section

In order to synthesize armchair graphene nanoribbons (AGNRs) without involving dehydrogenation, 1,4,5,8- tetrabromo-naphthalene (TBN) is used as the molecular precursor. The potential coupling sites along the growth direction to form 5-AGNRs were functionalized with bromine substituents, which may allow the necessary C-C bond formation after a thermal cleavage of C-Br bonds. A Au(111) substrate (Mateck GmbH, 9 mm in diameter, orientation accuracy better than 1º) was cleaned by cyclic Ar-ion sputtering and annealing in ultra-high vacuum (UHV) (base vacuum 3×10^{-10} mbar). TBN molecules were deposited onto this substrate by means of the organic molecular beam deposition (OMBD) technique. Low-temperature scanning tunnelling microscopy (LT-STM) (Omicron, base vacuum $<1\times10^{-10}$ mbar) working at 77 K after cooling with liquid N_2 was employed to investigate each sample prepared at various substrate temperatures. The STS measurements (dI/dV spectra) were performed using the lock-in technique.

All x-ray photoemission spectroscopy (XPS) experiments were carried out in a different UHV chamber (base vacuum $1x10^{-10}$ mbar). The XPS set-up consists of a monochromatic X-ray source providing Al Kα radiation ($\hbar\omega$ = 1486.6 eV) and a high-resolution hemispherical electron analyzer (Specs GmbH, Phoibos 150) for photoelectron detection. After introduction into the UHV system, the dedicated sample was annealed in situ by electron bombardment during XPS data acquisition. The particular sample temperature was measured by means of a thermocouple temperature sensor

attached to the sample holder of the manipulator.

Theoretical Section

Density Functional Theory (DFT) calculations were performed with the VASP code.[1-4] The projector augmented wave (PAW) method with a kinetic energy of 400eV was employed to describe the electron-ion interactions.[5,6] The generalized gradient approximation (GGA) with the Perdew-Burke-Ernzerhof (PBE) exchange-correlation functional was adopted to calculate the exchange and correlation energy.[7,8] For the unit cell, the Brillouin zone (BZ) sampling was done using a 2x2x1 Monkhorst-Pack grid for all calculations. The Au surface was modeled using periodic slabs, with four atomic layers and a vacuum thickness of 25 Å. The top-most two atomic layers of Au atoms and the AGNR were allowed to relax in three dimensions, while the bottom two layers of Au atoms were held fixed to the positions of bulk Au. The tolerance for the energy convergence is 10^{-5} eV. All structures are fully relaxed until the force on each atom is smaller than 0.01 eV per Å. The effect of van der Waals (vdW) interactions was included with the vdW-D2 method of Grimme. From the electronic ground-state structure, the STS spectroscopy and STM images were calculated with the Tersoff-Hamann approach and the Bardeen's method. The STM tip was modeled with a three-layer pyramid of tungsten on a four-layer W (100) film. [10-12]

Structural determination of the organogold compound

XPS measurements were carried out in order to confirm the chemical structure of the organogold compound proposed in Figure 1c. For this purpose, a dedicated sample of Au (111) with a TBN coverage of 1 ML was prepared and checked by STM right before the XPS experiment. Figure S1a shows the gradual change of the C1s region with increasing sample temperature. At room temperature (291 K, black curve), the C1s region clearly exhibits two components with binding energies of 285.3 eV and 284.2 eV, respectively. These components can be ascribed to two different carbon species corresponding to the C-Br bonds and the C-C bonds within a TBN molecule, respectively. As the temperature is increased to 320 K (blue curve), a remarkable decrease of intensity is observed for the peak centered at 285.3 eV, indicating a dissociation of the C-Br bonds. For higher temperatures, C-Br bond dissociation proceeds continuously until the respective component finally vanishes almost completely. Simultaneously, the second peak which is initially located at a binding energy of 284.2 eV gradually shifts to lower binding energies and reaches a minimum binding energy of 283.9 eV for a temperature of 342 K (green curve). However, this effect is reversed by further increasing the substrate temperature which eventually leads to an upward shift of the respective binding energy (red curve). In Figure S1b, the overall temperature-dependent behavior of the peak position is illustrated. The observed downward shift of 0.3 eV (from 284.2 eV to 283.9 eV) is considered to originate from the formation of C-Au bonds.[13] The opposite upward shift of 0.2 eV (from 283.9 eV to 284.1 eV), in turn, suggests a subsequent cleavage of the C-Au bonds which is accompanied by C-C bond formation due to polymerization during nanoribbon formation. Complementary to the C1s region, high-resolution XPS scans were recorded for the Br3d region for the same sample (see panel c and d, Figure S1). At room temperature (291 K, black curve in Figure S1c), only one bromine species

namely a Br3d spin-orbit split doublet at a binding energy of 69.8/70.8 eV is observed which can be ascribed to the presence of C-Br bonds. As the substrate temperature is continuously increased to 379 K (red curve), the intensity of this doublet gradually decreases which indicates the cleavage of C-Br bonds. On the other hand, simultaneously, an additional spin-orbit split doublet arises at a binding energy of about 67.9/68.9 eV. The associated energy shift of about 2 eV to lower binding energies with respect to the C-Br doublet is evidence of the temperature-induced formation of Br-Au bonds.[13] Finally, as it can easily be taken from Figure S1d, further annealing of the sample to temperatures up to about 450 K leads to a desorption of bromine from the surface in the course of nanoribbon formation. The crucial point is that the XPS data unambiguously verify the coexistence of Au-C and Au-Br bonds in a temperature range of about 340 − 370 K although a possible contribution of chemisorbed bromine atoms to the respective Br3d signal cannot be excluded. Thus, in combination with atomically resolved experimental STM data (Figure S1, panel e, I) as well as DFT-simulated STM images of the organogold compound (Figure S1, panel e, II, III), it can undoubtedly be noted that the organogold compound proposed in Figure1c indeed exists after the cleavage of C-Br bonds.

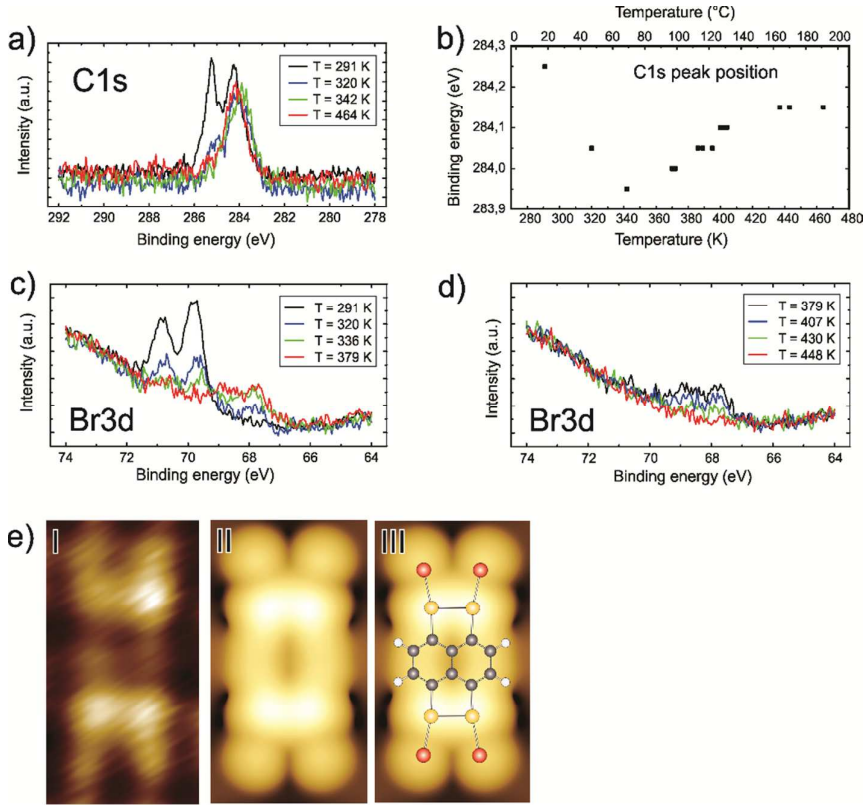

Figure S1 Comprehensive evidence for the structural determination of the organogold compound. a) XPS high-resolution scans of the C1s region for 1 ML TBN on Au (111) at sample temperatures of 291 K (black), 320 K (blue), 342 K (green), and 464 K (red). b) Binding energy of the C-C C1s component plotted against the sample temperature. c) XPS high-resolution scans of the Br3d region for the same sample at sample temperatures of 291 K (black), 320 K (blue), 336 K (green), and 379 K (red). d) XPS high-resolution scans of the Br3d region at temperatures of 379 K (black), 407 K (blue), 430 K (green), and 448 K (red). e) STM image (I) and DFT-simulated STM image

(II) of the organogold compound. The optimized geometric structure (Br: red, Au: yellow, C: black, H: white) is compared to the DFT-simulated STM image for clarity (III).

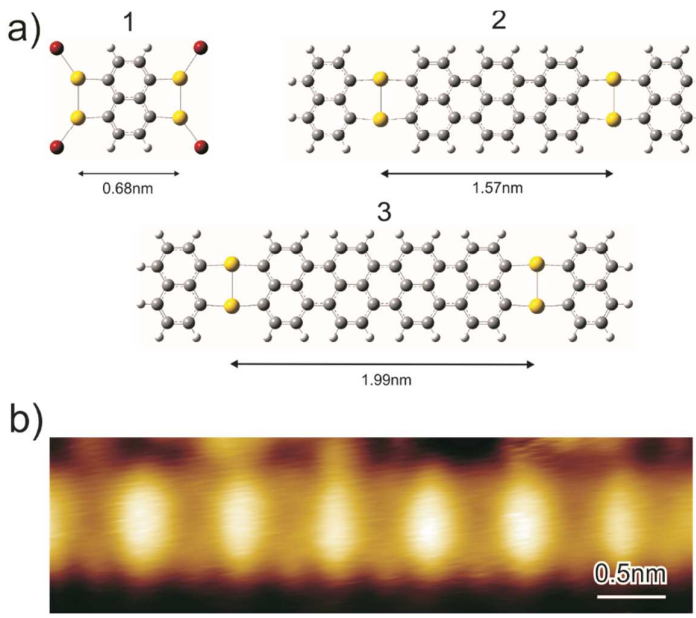

Figure S2 a) Optimized geometric structure of the organogold compounds nap-Au (1), tri-nap-Au (2) and tetra-nap-Au (3), each for the gas phase. DFT calculations at the level of B3LYP with a basis set of 6-31G for atoms of C, Br and H and lanl2dz for Au have been used. The length of the respective ribbon part between opposite Au atoms is determined to be 0.68 nm (nap-Au), 1.57 nm (tri-nap-Au) and 1.99 nm (tetra-nap-Au), respectively. b) High-resolution STM image of a long 'nodal ribbon'. The bright bumps with higher tunneling probability represent the position of gold atoms.

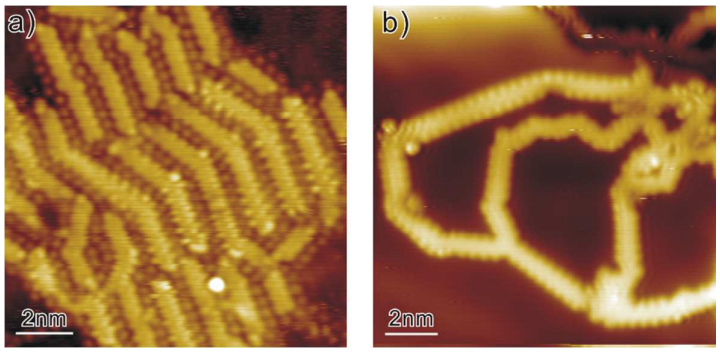

Figure S3 Desorption of Br adsorbate upon annealing in the high temperature regime a) STM image of 5-AGNRs with circumjacent Br adsorbate. b) STM image of 5-AGNRs upon annealing at a temperature of 570 K for ca. 5 mins showing no Br adsorbate on the surface.

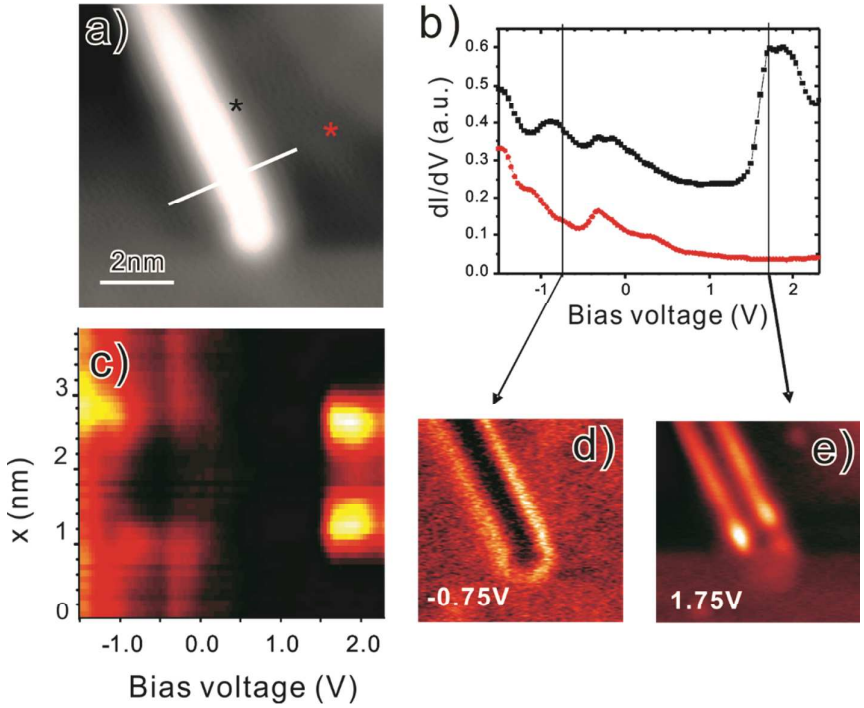

Figure S4 STS band gap measurements of 7-AGNRs. a) STM image of a 7-AGNR prepared on Au (111). b) STS curves obtained on bare Au (111) (red curve) and on the edge of the 7-AGNR (black curve). c) 2D STS map composed of 48 d*I*/d*V* curves which were recorded across the 7-AGNR (as marked by a white line in panel a). d), e) STS maps recorded at bias voltages of -0.75V (d) and 1.75V (e), respectively.

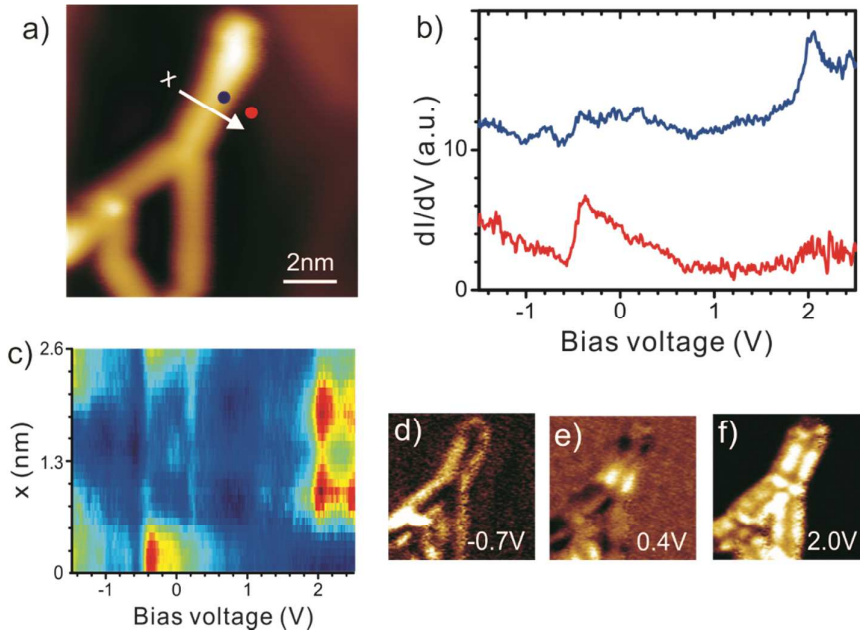

Figure S5 Supplementary example for an STS measurement on 5-AGNRs. a) STM image of a 5-AGNR. Blue and red dots mark, respectively, the positions where the STM tip is positioned for the STS measurement. b) d*I*/d*V* curves obtained on bare Au (111) (red curve) and on the edge of the 5-AGNR (blue curve). c) 2D STS map composed of 30 d*I*/d*V* spectra which were recorded

along the direction indicated by the white arrow in panel a. d) − f) d*I*/d*V* maps of the 5-AGNR obtained at bias voltages of -0.7 V (d), 0.4 V (e) and 2 V (f), respectively.

Further evidence for the determination of valence and conduction band edges

The valence and conduction band edges of 5-AGNRs on Au (111) were determined on the basis of a statistical analysis of all STS spectra obtained for various samples, tips and instruments. The distributions of the valence and conduction band edges are shown in Figure S6, panel a and b, respectively. The average energies of -0.69 eV and 2.09 eV for the valence band and conduction band edge, respectively, were derived from 90 selected d*I*/d*V* spectra which were mainly obtained for a tip position on top of the longitudinal edges of the 5-AGNRs. Although certain d*I*/d*V* spectra occasionally exhibit additional features, either on the edge sides (panel c, I,II,III) or on the main body of the ribbon (IV), the resonances at -0.69 V and 2.09 V are always discernible, as shown in Figure S6, panel c. In any case, 2D d*I*/d*V* maps of the electronic state at 2.09 eV show a high intensity on the longitudinal edges without nodal features. However, occasionally, additional nodal features appear on d*I*/d*V* maps for a sample bias of -0.7 V (see Figure 3, panel d). These features might originate from defects, e.g. the bent shape of a ribbon as shown in Figure 3d. In all other cases, d*I*/d*V* mapping for a sample bias of -0.7 V reveals a consistent distribution of enhanced intensity on the longitudinal edges of the ribbon (Figure S6, panel d, II). Accordingly, the electronic states at -0.69 eV and 2.09 eV are attributed to the valence and conduction band edge, respectively.

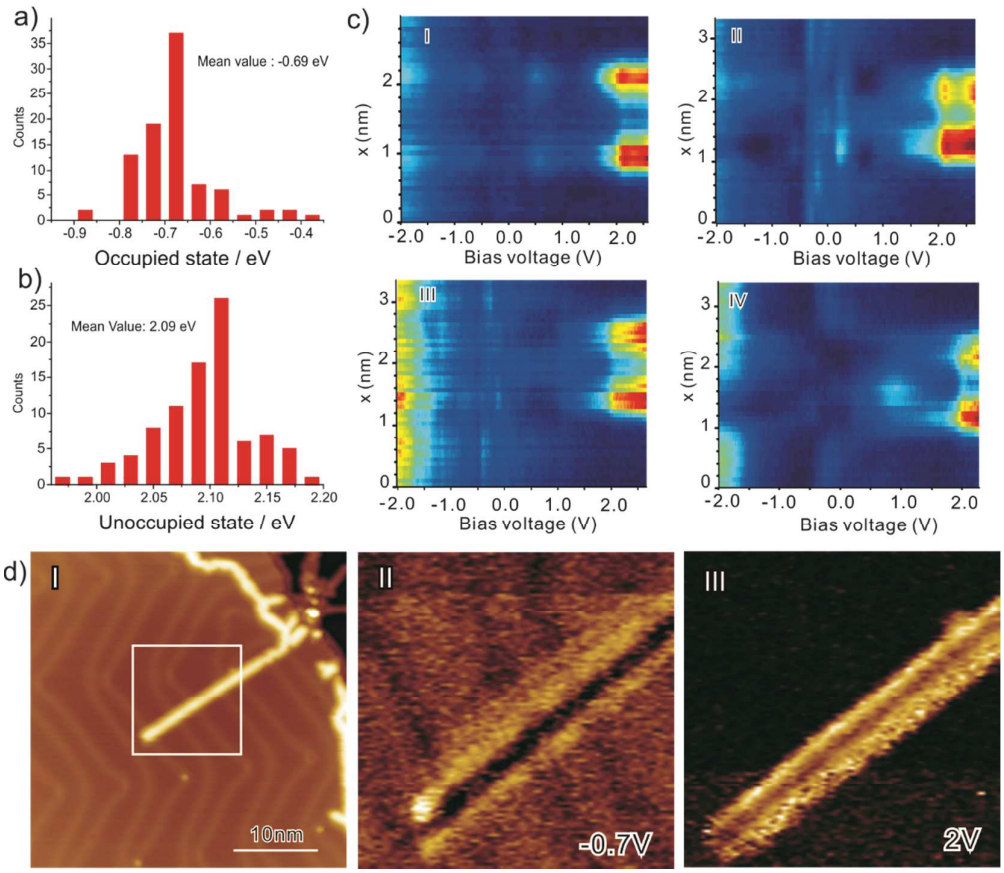

Figure S6 Supplementary STS data for the determination of the electronic structure of 5-AGNRs on Au (111). The statistical distribution of the valence (a) and the conduction (b) band edge is derived from 90 selected d*I*/d*V* spectra which were mainly collected on the longitudinal edges of 5-AGNRs. Note that the selected d*I*/d*V* spectra were acquired by using various samples, tips and instruments. c) 2D STS map composed of multiple (30 − 50) d*I*/d*V* spectra taken across various ribbons. Occasionally, additional spectral features appear in the d*I*/d*V* spectra, e.g. at bias voltages of 0.7 V (I), 0.25 V (II), -0.1 V (III), and 1.0 V (IV). However, the valence and conduction band edges, corresponding to the resonances at -0.69 V and 2.09 V, respectively, are always discernible. d) STM image of the longest 5-AGNRs observed experimentally (I) and corresponding 2D d*I*/d*V* maps for bias voltages of -0.7 V (II) and 2 V (III), respectively, showing a consistent distribution of enhanced intensity on the longitudinal edges of the ribbon.

DFT simulation of the adsorption-induced band gap widening

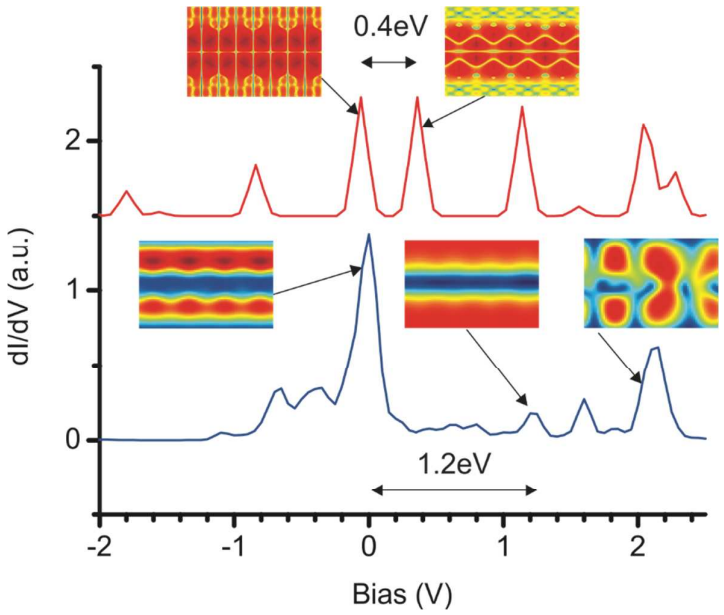

Figure S7 d*I*/d*V* spectra of a 5-AGNR in immediate proximity to (blue curve) and located 8 Å above (red curve) a Au (111) surface as calculated by DFT. In analogy to the STM experiment on 5-AGNRs adsorbed on Au (111), a tungsten tip was assumed in order to simulate the d*I*/d*V* spectra. Furthermore, the STM tip was assumed to be positioned above the edge of the ribbon.

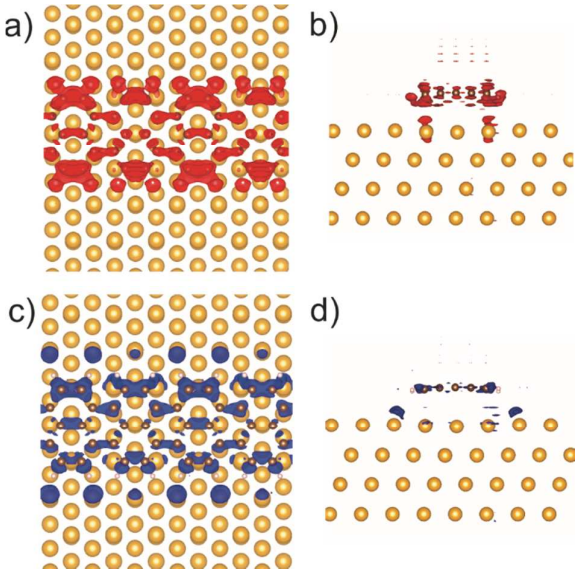

Figure S8 Charge difference calculations for a 5-AGNR adsorbed on a Au (111) substrate. Apparently, a specific distribution of the electron charge of the 5-AGNR is induced by the underlying substrate. a), b) Top and side view of an isosurface of 0.001 electrons/$Å^3$ (shown in red). c), d) Top and side view of an isosurface of -0.001 electrons/$Å^3$ (shown in blue).

As shown in Figure S7, the calculated HOMO-LUMO gap for a 5-AGNR supported by a Au (111) surface is determined to 1.2 eV for a tungsten STM tip (the Fermi level has been aligned with the HOMO of the GNR). In consideration of the respective spatial distribution, the calculated HOMO and LUMO energies are in good agreement with the experimental observations. However, in case the nanoribbon is decoupled from the Au surface, i.e. being located in a distance of 8 Å above the surface, the HOMO-LUMO gap is reduced to around 0.4 eV, which is consistent with the HOMO-LUMO gap of a 5-AGNR in the gas phase. The band gap widening is ascribed to a hybridization of the molecular states of the 5AGNR with the surface states of the underlying substrate.

In order to verify this hybridization effect, charge difference calculations have been carried out which are based on the following equation:

$$\text{Charge (CHG)} = \text{CHG}_{\text{iso-G}} + \text{CHG}_{\text{iso-Au}} - \text{CHG}_{\text{G-Au}}$$

Here, $\text{CHG}_{\text{iso-G}}$ and $\text{CHG}_{\text{iso-Au}}$ denote the electron charge of an isolated 5-AGNR and the isolated Au (111) substrate in vacuum, respectively. The parameter $\text{CHG}_{\text{G-Au}}$, on the other hand, stands for the electron charge of a 5-AGNR adsorbed on the Au(111) substrate. As depicted in Figure S8, the charge difference calculations demonstrate the occurrence of a charge transfer within the 5-AGNR as well as from the 5-AGNR to the Au(111) substrate, in particular to the Au atoms of the rows adjacent to the longitudinal edges of the ribbon. The charge difference calculation, therefore, confirms the hybridization of surface states of the substrate with molecular states of the adsorbate.

Synthesis and characterization of 1,4,5,8-tetrabromo-naphthalene (TBN)

1M NaOH was added to a suspension of 1,4,5,8- naphthalenetetracarboxylic acid dianhyride (4.00 mmol) in 20 ml water. The mixture was stirred in order to obtain a limpid solution of tetra sodium salt. Bromine (1.0 ml, 3.11 g) was added in one portion and the reaction mixture was stirred at 90 °C for 24 h. The precipitate was filtered and dried. The crude solid was extracted with dichloromethane. The organic solvent was evaporated to dryness and the residue was purified by column chromatography using hexane as eluent on silica, the yield being 180 mg (10%).

1,4,5,8-tetrabromonaphthalene

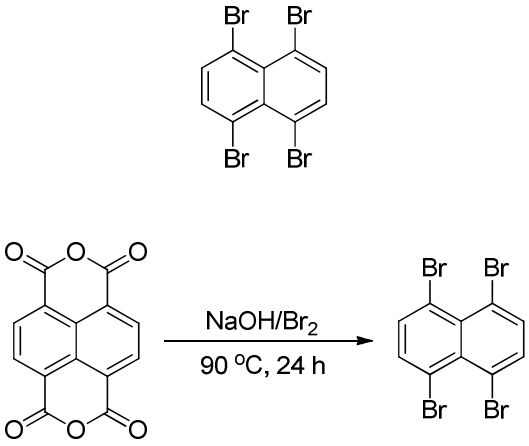

FD-Mass: calc.: 443.75 found: 444.0

^{1}H-NMR (δ (ppm), CD_2Cl_2): 7.74 (s, 4H, CH);.

^{13}C-NMR (δ (ppm), CD_2Cl_2): 120.03 (4C, CBr); 132.97 (2C, C); 135.39 (4C, CH).

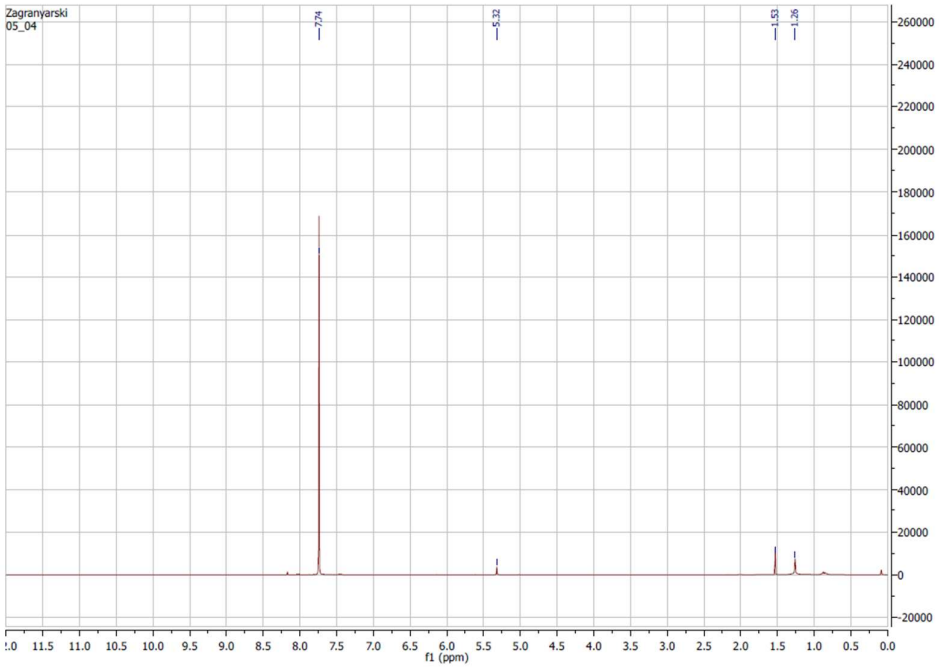

Figure S9. 1H NMR spectrum of TBN in CD_2Cl_2.

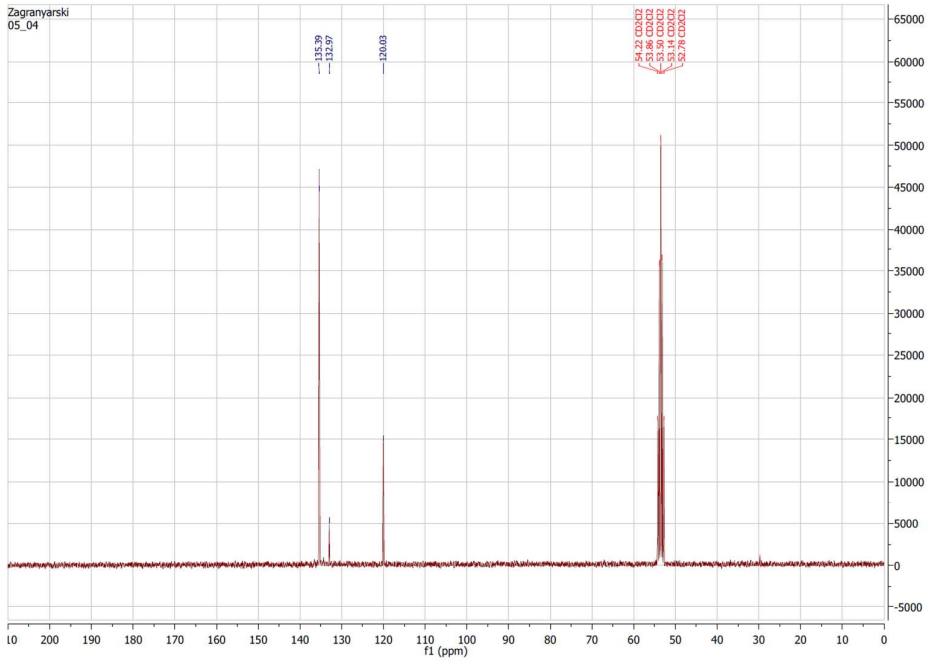

Figure S10. 13C NMR spectrum of TBN in CD_2Cl_2.

References:

(1) Kresse, G.; Furthmuller, J. *Phys. Rev. B***1996**, *54*, 11169.

(2) Kresse, G.; Furthmuller, J. *Comp. Mat. Sci.***1996**, *6*, 15.

(3) Kresse, G.; Hafner, J. *Phys. Rev. B***1993**, *47*, 558.

(4) Kresse, G.; Hafner, J. *Phys. Rev. B***1994**, *49*, 14251.

(5) Blochl, P. E. *Phys. Rev. B***1994**, *50*, 17953.

(6) Kresse, G.; Joubert, D. *Phys. Rev. B***1999**, *59*, 1758.

(7) Perdew, J. P.; Burke, K.; Ernzerhof, M. *Phys. Rev. Lett.***1996**, *77*, 3865.

(8) Perdew, J. P.; Burke, K.; Ernzerhof, M. *Phys. Rev. Lett.***1997**, *78*, 1396.

(9) Monkhorst, H. J.; Pack, J. D. *Phys. Rev. B***1976**, *13*, 5188.

(10) Bardeen, J. *Phys. Rev. Lett.* **1962**, *9*, 147.

(11) Hofer, W. A.; Foster, A. S.; Shluger, A. L. *Rev. Mod. Phys.***2003**, *75*, 1287.

(12) Lin, H.; Rauba, J. M. C.; Thygesen, K. S.; Jacobsen, K. W.; Simmons, M. Y.; Hofer, W. A. *Front. Phys. China* **2010**, *5*, 369.

(13) Batra, A; Cvetko, D.; Kladnik, G.; Adak, O.; Cardoso, C.; Ferretti, A.; Prezzi, D.; Molinari, E.; Morgante, A.; Venkataraman, L. *Chem. Sci.*, **2014**, *5*, 4419.

(14) Deng, Z.; Lin, H.; Ji, W.; Gao, L.; Lin, X.; Cheng, Z.; He, X.; Lu, J.; Shi, D.; Hofer, W.; Gao, H. J. *Phys. Rev. Lett.* **2006**, *96*.